Macromolecular Materials and Engineering
Open Access
www.mame-journal.de

Thermal and Rheological Properties of Fischer–Tropsch Wax/High-Flow LLDPE Blends

*Thobile Mhlabeni, Shatish Ramjee, Jorge López, Ana-María Díaz-Díaz, Ramón Artiaga, and Walter Focke**

Waxes find use as processing aids in filled compounds and polyethylene-based masterbatches. In such applications, the thermal and physical property changes they impart to the polymer matrix are important. Therefore, this study details results obtained for blends prepared by mixing a Fischer–Tropsch (F–T) wax with a high-flow linear low-density polyethylene (LLDPE). The melting and crystallization behavior are studied using hot-stage polarized optical microscopy (POM) and differential scanning calorimetry (DSC). The calorimetry results are consistent with partial cocrystallization of the two components. The melting and crystallization exo- and endotherms for the wax- and LLDPE-rich phases remained separate. However, they change in shape and shift toward higher- and lower temperature ranges, respectively. It is found that increasing the wax content delays the crystallization, decreases the overall crystallinity, and reduces the size of the crystallites of the polyethylene-rich phase. Rotational viscosity is measured at 170 °C in the Newtonian shear-rate range. The variation of the zero-shear viscosity with blend composition is consistent with the assumption of a homogeneous melt in which the chains are in an entangled state. Therefore, it is concluded that the wax and LLDPE are, in effect, miscible in the melt and partially compatible in the solid state.

1. Introduction

Wax/polyethylene blends continue to be studied as phase-change thermal energy storage materials.[1] Their use as processing aids (PA), in the preparation of masterbatches for large volume plastics applications, is also important but it has received less attention.[2] The present study forms part of larger investigation addressing the performance of waxes in the latter application. For that purpose, an important aspect is the phase structures present in both the melt and in the solid states. Therefore, this study reports on the properties of a blend comprising a low molecular mass Fischer–Tropsch (F-T) wax with a high-flow linear-low density polyethylene (LLDPE).

Several studies investigated the phase structures and properties of the wax/polyethylene blends in both the melt and in the solid states. Sotomayor, Krupa[3] investigated the compatibility between paraffin wax and high-density polyethylene (HDPE). They observed the presence of two distinct tan δ peaks in dynamic mechanical analysis (DMA). This indicated a biphasic amorphous structure consistent with immiscibility or at best partial miscibility in the solid state. Others, studying similar blends, probed the miscibility in the crystalline phase domains.[4–7] This type of miscibility requires that a degree of cocrystallization must occur. Chen and Wolcott[5,6] investigated the solid phase morphology of octadecane blends with HDPE, low-density polyethylene (LDPE), and LLDPE. Atomic force microscopy revealed phase-separated crystalline morphologies while differential scanning calorimetry (DSC) measurements indicated two distinct crystallization exotherms. Furthermore, separate melting and crystallization events were observed in temperature-scanned DSC thermograms. These corresponded closely with those of the neat components which implies, at best, partial miscibility in the solid state. Gumede, Luyt[7] also found two distinct crystallization exotherms in a 30/70 wax/LLDPE composite. In contrast, Mpanza and Luyt,[4] reported a single endothermic melting peak for LLDPE blends containing less than 10 wt% of a range of different waxes. Such behavior is consistent with miscibility of the constituents in both the melt and in the solid state. Gumede, Luyt[7] attributed the shifts in the melting and crystallization onset temperatures of the LLDPE-rich phase to cocrystallization phenomena. This was supported by small-angle X-ray scattering (SAXS) results. They observed the development of a new SAXS peak which was associated with the formation of a wax-rich phase featuring a higher melting

T. Mhlabeni, S. Ramjee, W. Focke
Institute of Applied Materials
Department of Chemical Engineering
University of Pretoria
Private Bag X20, Hatfield 0028, South Africa
E-mail: walter.focke@up.ac.za
J. López, A.-M. Díaz-Díaz, R. Artiaga
Naval and Industrial Technologies Research Center
The University of A Coruña
Ferrol Industrial Campus
Ferrol 15403, Spain

The ORCID identification number(s) for the author(s) of this article can be found under https://doi.org/10.1002/mame.202300125

DOI: 10.1002/mame.202300125

temperature. Most of the above-mentioned studies also reported melting point depression of the polyethylene-rich phase. This held irrespective of the polyethylene type, i.e., whether HDPE, LDPE, or LLDPE.[5,6]

The rheological behavior of polymers is significantly affected by the molecular mass. The rheology of the viscosity of polymer melts is sometimes studied using rotational rheometry. Such data can complement more direct measurements of molecular mass by techniques such as gel permeation chromatography or membrane osmometry.[8] Typically, polymer melts approach Newtonian behavior as the shear rate approaches zero. The viscosity becomes independent of shear rate and it is denoted the zero-shear viscosity. The zero-shear viscosity depends on the measurement temperature, the structure of the polymers present and the molecular mass distribution.[9] Sotomayor, Krupa[3] studied the rheology of blends of HDPE with a soft paraffin wax at high shear rates and a temperature of 160 °C. They observed that the results followed a linear blending rule for the logarithms of the pure components. This was interpreted as indicating complete miscibility in the molten state. Positive and/or negative deviations from the logarithmic additive rule has been linked to immiscibility within such blend systems. However, partial miscibility was also associated with such behavior. Liu, Wang[10] considered the composition dependence of the zero-shear viscosity LLDPE/HDPE and LLDPE/LDPE blends. Deviations from the logarithmic mixing rule were attributed to factors associated with the molecular mass of the blend components.[11]

In the present study, a low molecular mass commercial F–T wax was melt-blended with a high-flow LLDPE grade. DSC, polarized optical microscopy (POM), and dynamic rheological measurements in the melt-state and solid-state were performed covering a wide range of compositions. These techniques were used to probe the microstructure of the wax/LLDPE system in the molten- and solid states. The objective was to gain a better understanding of the overall phase behavior of the F–T wax/LLDPE blend system. The wax is primarily constituted of linear alkanes but some linear alkenes are also present. In contrast, the linear low-density polyethylene features numerous short branches due to the incorporation of higher alpha-olefins as comonomers. These differences have implications with respect to compatibility in the solid state but this aspect was not investigated in the present study. Both components feature alkane-like backbones albeit differing in geometry. However, the LLDPE might contain fractions with lower branching and it is also possible for some of the chains to have long polyethylene sequences, i.e., linear intramolecular portions. Nevertheless, the similarity in intermolecular forces and melt phase chain mobility allowed revisiting the theoretical and empirical expressions that link the zero-shear viscosity with blend composition.

The present manuscript builds upon previous work conducted by Mhlabeni et al.,[12] which introduced a new experimental F-T wax. In comparison to the previous study, the current research aims to deliver the Supporting Information regarding the compatibility and viscosity characteristics of this F–T wax. In particularly, the F–T wax utilized in this study has an even lower molecular weight than the one investigated in the previous research. The primary objective of this work is to address the limitations associated with the molecular weight of the F–T wax. In addition to investigating the compatibility and viscosity, this manuscript also introduces a novel approach to the analysis of the DSC isothermal study. The methodology involves scaling and subtracting the baseline to suppress the ramp-to-iso artifact, which is a significant contribution to the field. This approach ensures more accurate and reliable results in the DSC analysis. Furthermore, the manuscript presents a unique analysis of rheology data, which has not been applied to mixtures of this nature before. This analysis provides valuable insights into the behavior and properties of the F–T wax in different conditions. All these contributions aim to advance the understanding of F–T wax properties and facilitate its practical applications as a processing aid.

2. Results and Discussion

2.1. Crystalline Morphology from Hot-Stage Microscopy

Figure 1 shows the crystalline morphology of the wax/LLDPE blends at selected temperatures as revealed by hot-stage polarized optical microscopy. The image in Figure 1a represents the neat wax at a temperature of 65 °C. It reveals a crystalline morphology featuring fine, needle-like structures. Figure 1b–f shows the crystalline morphologies observed at 100 °C for selected blends. The dark colored background represents a molten liquid region in which vibrantly colored crystalline regions are observable. Adding even small amounts of LLDPE to the wax, results in a transition away from the wax needle-like texture toward that of a fine "mosaic"-like texture. This is likely caused by higher nucleation rates which lead to rapid impingement of the growing crystal domains. LLDPE-rich samples feature the distinctive "Maltese cross" pattern found for the spherulitic crystallization of polyethyelene.[13] Closer inspection also revealed the presence of banded structures typically observed for polyethylene.[14] These observations agree with the phase images reported by Chen and Wolcott[6] for paraffin wax/LLDPE blends. The slight colorization found in the amorphous fraction, which is prominent in the 30/70 blend, may be indicative of crystalline regions that are at a depth beyond the focal length.

As the wax fraction increased to 50 wt%, the LLDPE spherulitic domains decreased in size. Eventually a point, observable in Figure 1b,c, is reached where they could not be distinguished at the magnification employed. **Table 1** lists estimates for the observed spherulite diameters. The decrease in size, at higher wax fractions, appears to be caused by enhanced nucleation.

2.2. LLDPE Equilibrium Temperature-Isothermal Process

The Hoffmann–Weeks equation[15,16] for the lamellar thickness was used to estimate the ultimate equilibrium melting temperature of the LLDPE

$$T_m = T_c/\beta + (1 - 1/\beta)\, T_m^o \quad (1)$$

where the parameter β represents the lamellar thickening ratio which links the experimentally determined isothermal crystallization temperature, T_c, to the melting temperature, T_m, and the equilibrium melting point, T_m^o. According to this equation, a plot of T_m against T_c should yield a straight line with slope

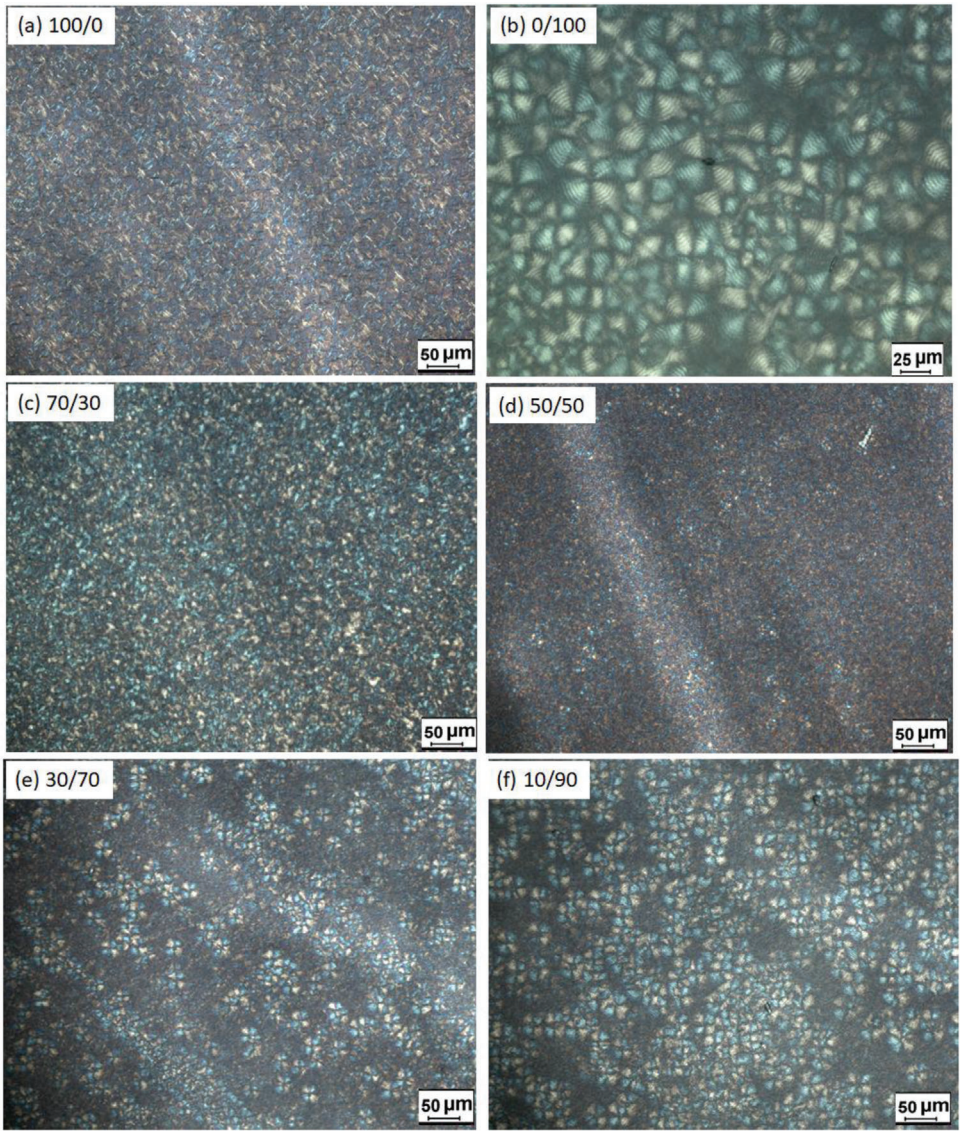

Figure 1. Polarized optical microscopy images of a) pure wax at 65 °C, b) pure LLDPE at 100 °C, and c–f) blends micrographed at a temperature of 100 °C at different wax/LLDPE mass ratios.

Table 1. Mean spherulite diameters (d), equilibrium melting temperature (T_m^o), and lamellar thickness ratio (β) found on isothermal LLDPE crystallization of wax/LLDPE blends.

Wax	wt%	80	60	50	30	20	10	0
d	µm	—	—	10.08 ± 0.03	15.83 ± 0.10	19.54 ± 0.07	23.17 ± 0.09	33.21 ± 0.20
T_m^o	°C	125.3	128.6	126.8	127.7	131.9	135.4	136.9
β	—	1.08	1.11	1.09	1.17	1.10	1.10	1.12

$1/\beta$ and intercept $(1 - 1/\beta)T_m^o$. The ultimate equilibrium melting temperature is obtained as the intersection of the straight-line plot of T_m against T_c with the line defined by $T_m^o = T_c$. It is important to note that, the Hoffmann–Weeks equation is based on the assumption that the difference between the isothermal crystallization temperature and observed melting temperature only depends on the thickness of the lameller formed during isothermal crystallization. In effect, Equation (1) defines the relationship between T_m^o in response to the crystallization temperature of a given system.[17] **Figure 2** shows this relationship in a form of linear plots generated from the data obtained from the hot stage optical microscopy studies. The estimated equilibrium melting

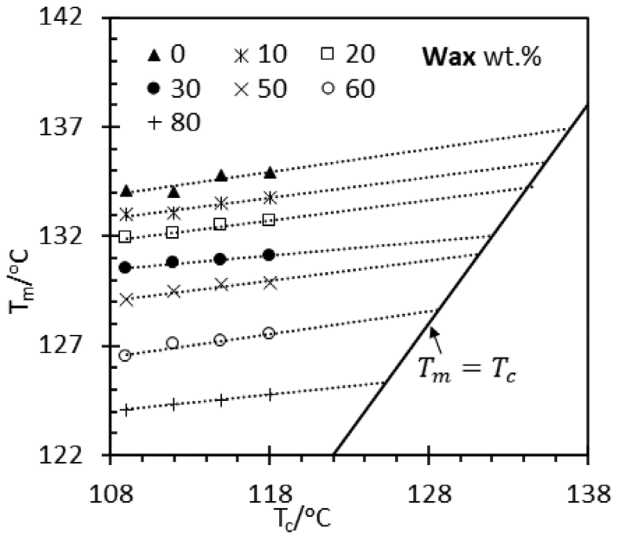

Figure 2. Ultimate equilibrium melting temperature of LLDPE spherulites formed at various wax/LLDPE blend compositions as determined from the hot stage optical microscopy data.

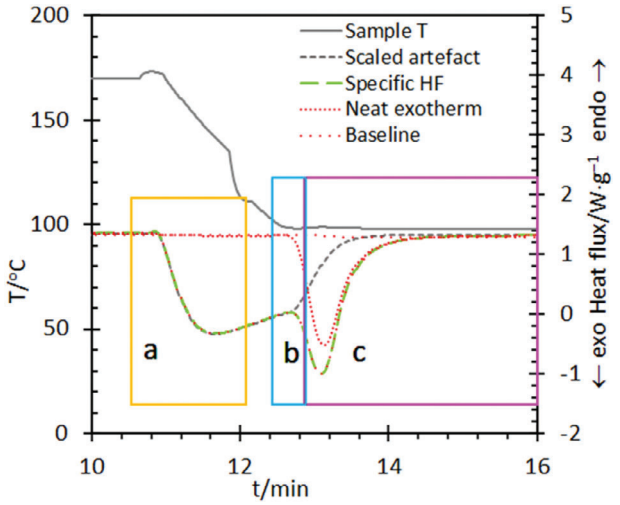

Figure 3. Illustration of the areas of the curves considered for the different fitting steps.

temperatures, with the corresponding lamellar thickening ratio's, are listed in Table 1. Increasing the wax fraction in the blends significantly depressed the equilibrium melting temperature of the LLDPE. Interestingly, the thickening ratio was essentially the same for all the blends studied. This suggests that the dynamics of the lamellar thickening ratio of crystal structure was preserved, while the equilibrium melting temperature varied with the blend composition as expected for a colligative property, i.e., the melting point depression.

2.3. Isothermal Crystallization Kinetics

Figure 3 displays a typical DSC trace obtained from a representative wax/LLDPE blend. The figure shows that the crystallization exotherm labelled as specific heat flow (HF) partially overlaps with an artefact resulting from the change from cooling to

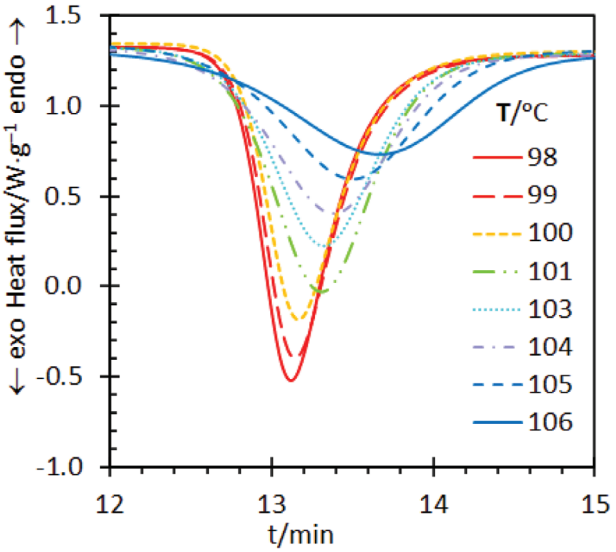

Figure 4. Isothermal crystallization curves of wax/LLDPE 30/70 blend composition at different values of T_c.

isotherm. It is clear that the conveniently scaled artefact perfectly matches the left part of the specific HF curve. It is also observed that there is a little change on the baseline that results from the crystallization as the heat capacity of the crystal is lower than that of the amorphous phase. A vertical line marks the beginning of the isothermal condition. It can be observed on the temperature curve that a tiny overheating is produced as a consequence of the exothermic process. Thus, before doing any kinetic analysis, the artefact was removed from the bulk DSC data as follows: taking as a reference Figure 3, the "a"-labeled part of the specific HF curve clearly corresponds to the aforementioned artefact and is well separated from the crystallization peak. Thus, we can assume that this part practically corresponds to the artefact. This part of the specific HF curve is vertically shifted for baseline matching and fitted by the artefact multiplied by a scale factor (sf). It can be observed that the matching of both curves is nearly perfect until a divergence appears in region "b," where the effect of crystallization begins to be evident. The neat exotherm curve region "c" obtained by the removal of the scaled artifact is also displayed on the same figure.

Figure 4 displays neat DSC traces, resulting from the removal of the artefact, showing the selected isothermal crystallization temperature for a blend containing 30wax/70LLDPE wt%. The shape of the crystallization exotherms curves were determined by the mode of the nucleation process, the subsequent crystal growth kinetics and finally also by the effect of spherulites impinging on each other. Figure 4 indicates that the exotherm peaks shifted to later times with increasing crystallization temperature. Therefore, complete crystallization of the LLDPE phase in the 30/70 wax/LLDPE blend composition is achieved within shorter times as the crystallization temperature is reduced.

Clearly, the temperature significantly affected the crystallization kinetics of the LLDPE polymer. The log-logistic distribution provides an alternative expression to represent the crystallization process.[18] In addition, there is a method based on generalized

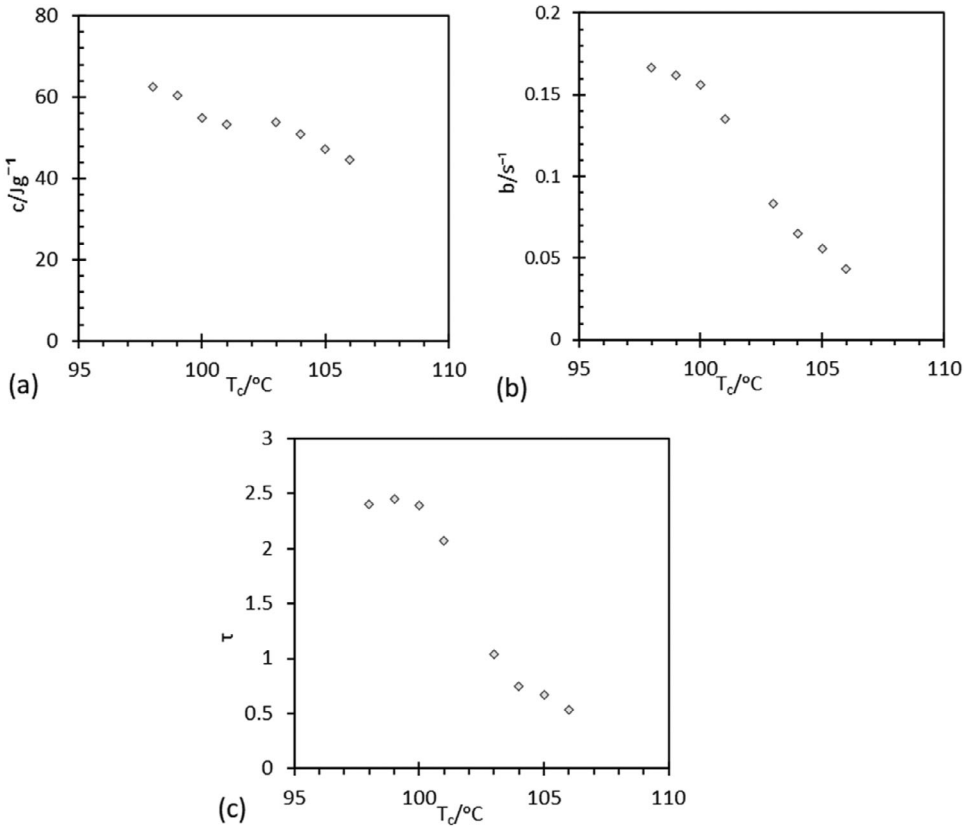

Figure 5. Plots of the logistic fitting parameters a) crystallization enthalpy versus the crystallization temperature, b) *b* parameter versus the crystallization temperature, and c) τ versus the crystallization temperature.

logistics which allows for very good fittings of polymer crystallizations in different contexts.[19]

The method applied here consisted of fitting each individual crystallization isothermal DSC curves by a mixture of a time-derivative generalized logistic function (DGL), which accounts for the crystallization exotherm, and a generalized logistic function (GL) multiplied by a scale factor, which account for the change of heat flow along the process

$$y_{\text{fit}}\ (\text{t}) = y_2\ (\text{t}) + sf \cdot y_1\ (\text{t}) \tag{2}$$

where $y_1(t)$ and $y_2(t)$ represents GL and DGL, respectively. GL and DGL share the rate and the symmetry parameters and the time location of the maximum. Thus, GL and DGL are synchronized as both enthalpy and heat capacity, *Cp*, changes that come from the same crystallization process

$$y_1\ (t) = \frac{1}{\left(1+\tau \cdot \exp\left(-b \cdot \left(t_{\text{apm}} - t\right)\right)\right)^{1/\tau}} \tag{3}$$

$$y_2\ (t) = \frac{c \cdot b \cdot \exp\left(-b \cdot \left(t_{\text{apm}} - t\right)\right)}{\left(1+\tau \cdot \exp\left(-b \cdot \left(t_{\text{apm}} - t\right)\right)\right)^{(1+\tau)/\tau}} \tag{4}$$

where t_{apm} is the time at the peak maximum, *c* represents the area of the peak, τ is the symmetry factor, where $\tau = 1$ means perfect symmetry and *b* is a rate factor which depends on temperature. The baseline-change along the transition, which comes from the change of *Cp* along the crystallization process, is represented by the product of y_1 by a scale factor, ΔHF, which is the difference of heat flow as measured from $t = 10$ min to $t = 16$ min. After several trials, it was found that the shape of the artifact curve in the "b"-region of Figure 3 is not very reproducible. A small anticipation or delay with respect to the specific HF drop in that area may lead to important distortions of the calculated specific HF curve. Consequently, the data contained in the "b"-region were disregarded and only the specific HF exotherm data contained at the "c"-region were used for the fitting through Equation (4) by minimizing the average squared error (ASE). For this fitting, we used the ΔHF scale factor as a fixed parameter. The fitting parameters were t_{apm}, *c*, *b*, and τ. **Figure 5** plots how the fitting parameters depend on the crystallization temperature. It is observed that the area of the peak, represented by *c*, slightly decreases as the crystallization temperature increases. That suggests that perhaps some of the lowest molecular mass fractions fail to crystalize when the crystallization temperature is increased. On the other hand, parameter *b* and τ follow a shape that looks like half a bell, generally decreasing as the temperature increases above 100 °C. According to Equation (2), tau = 1 represents a perfect symmetry of the crystallization rate around the central temperature (in this case about 103 °C). On the other hand, Equation (6) shows that the apparent reaction order is tau+1. In this case, it means a reaction order of 2. The fact that *b* and τ follows similar trends with temperature suggests that a higher *b* value is obtained with a higher

Table 2. Parameter values of the fitting of the *b* parameter values by Equation (5).

b Parameters		
t_{cryst} [s]	T_{cent} [°C]	T_{hwhm} [°C]
355.9	97.8	5.6

reaction order, that is, when a higher number of "species" are contributing to the crystallization process. It is well known that the crystallization rate follows a bell-shaped trend decreasing both sides toward the glass transition temperature and to the melting temperature.[20,21] Thus, following a similar approach than in a previous work, the *b* values were fit to a Gaussian function[19]

$$b\ (T) = \frac{1}{t_{cryst}} \cdot \exp\left(-ln\,(2) \cdot \left(\frac{T - T_{cent}}{T_{hwhm}}\right)^2\right) \quad (5)$$

where t_{cryst} represents a crystallization time, T_{cent} the temperature at which the maximum rate is obtained, and T_{hwhm} the half width at height maximum, which is related to how *b* decreases as *T* diverges from T_{cent}. According to this expression, the rate parameter is dependent on a characteristic temperature and characteristic crystallization time, which are specific for a given crystal structure. The values resulting from the fit are displayed on **Table 2**. Accordingly, the temperature at which the LLDPE can crystallize at its highest crystallization rate is about 97.8 °C. The crystallization rate of this form was found to be 355.9 s which decreases to the half of its maximum when moving 5.6 °C up or down from the central value. **Figure 6**a,b shows how the experimental data fit into a Gaussian distribution of the crystallization rate versus crystallization temperature. The equivalent crystallization times are also plotted. It is observed that the higher the distance to the central temperature, the higher the effect of a change in temperature on the time to crystallize.

On the other hand, τ, which represents the symmetry of the peak, can be assimilated to a reaction order since Equation (4) can be rewritten as a function of the conversion

$$d\alpha/dt = c \cdot b \cdot \exp\left[-b \cdot \left(t_{apm} - t\right)\right] \cdot [(1-\alpha)]^{1+\tau} \quad (6)$$

where α is the conversion. The idea that crystallization from the melt can be assimilated to a reaction order process would not be meaningless given that it is at intermediate temperatures, of maximum crystallization rate, where a greater number of interactions of nucleation and crystal growth phenomena are expected to occur.

2.4. Nonisothermal Melting and Crystallization Process

The nonisothermal DSC thermograms in **Figure 7** show the melting and crystallization behavior of the neat components as well as the blends. The melting and crystallization peak temperatures of the wax were 60.4 and 47.0 °C respectively. The corresponding values for the LLDPE were 125.6 and 103.0 °C, respectively. The blend containing 10 wt% wax did not feature melting or crystallization peaks that could be attributed to a wax phase. This is indicative of miscibility.

Furthermore, one can observe significant variations in the melting and crystallization curves of the experimental data, Figure 7, in comparison to mass-based linear blending calculated data for four selected blends, **Figure 8**. The melting peak temperatures of the wax-rich phase remains constant, while the crystallization peak temperature slightly increases; but both these peaks are also observed to broaden in the direction of increasing temperature. In addition, a developing shoulder-peak during crystallization of wax was observed on both Figures 7 and 8. This may be indicative of a slower relaxation due to interaction with polymer chains. On the other hand, both the melting and crystallization peak temperatures of the LLDPE-rich phase decrease considerably with increasing wax concentration. Similar results were previously reported.[22–23,25] They were attributed to partial miscibility in the solid state, i.e., incorporation of the wax in LLDPE crystallites. Furthermore, LLDPE melting peak splits into two low and high melting peaks, forming a bimodal peak. This is consistent with a portion of the polymer cocrystallizing with the wax.

Plots of the melting peak temperatures of the wax and LLDPE are shown in **Figure 9** for the blends of different compositions. Significant melting-point depression of the LLDPE-rich phase is evident, while the melting-point of the wax-rich phase appears to be largely unaffected. Above the melting temperature of the

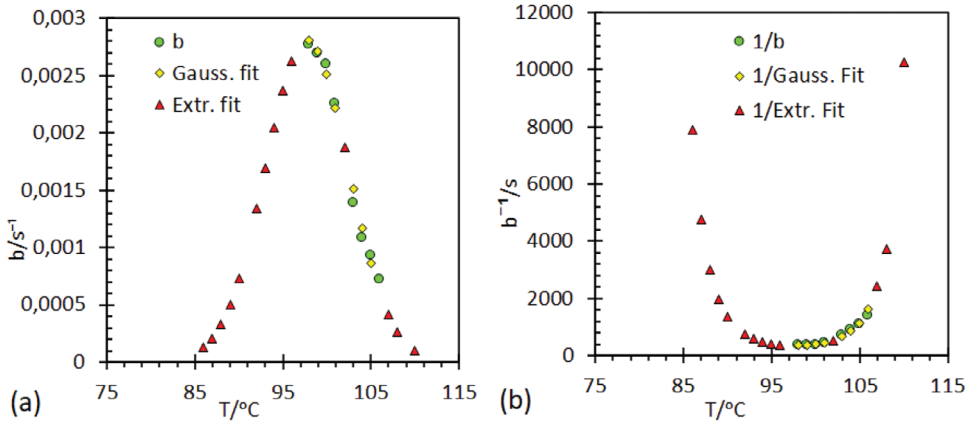

Figure 6. Fit of the *b* parameters versus the crystallization temperature by a) a Gaussian function and the b) equivalent crystallization times.

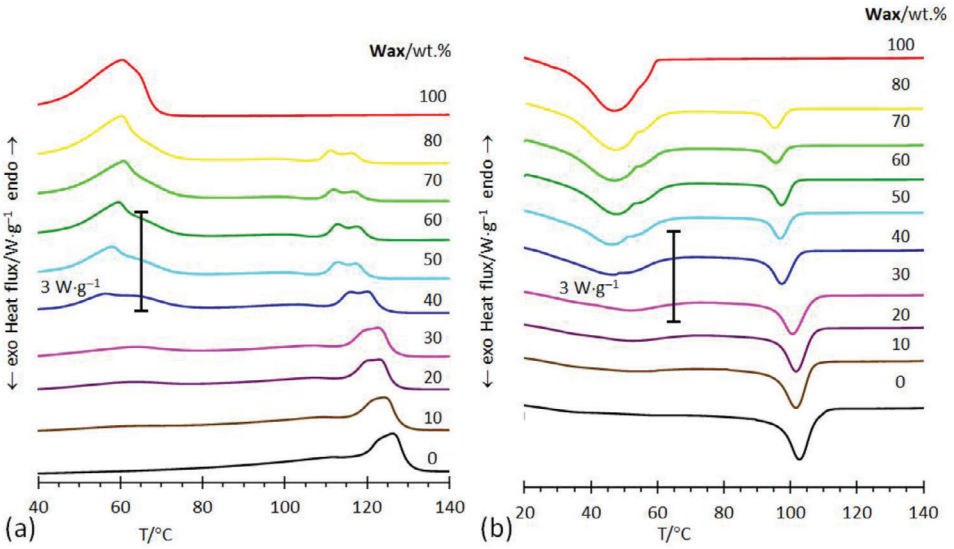

Figure 7. Plot of a) Melting and b) crystallization curves of wax/LLDPE at various blend compositions.

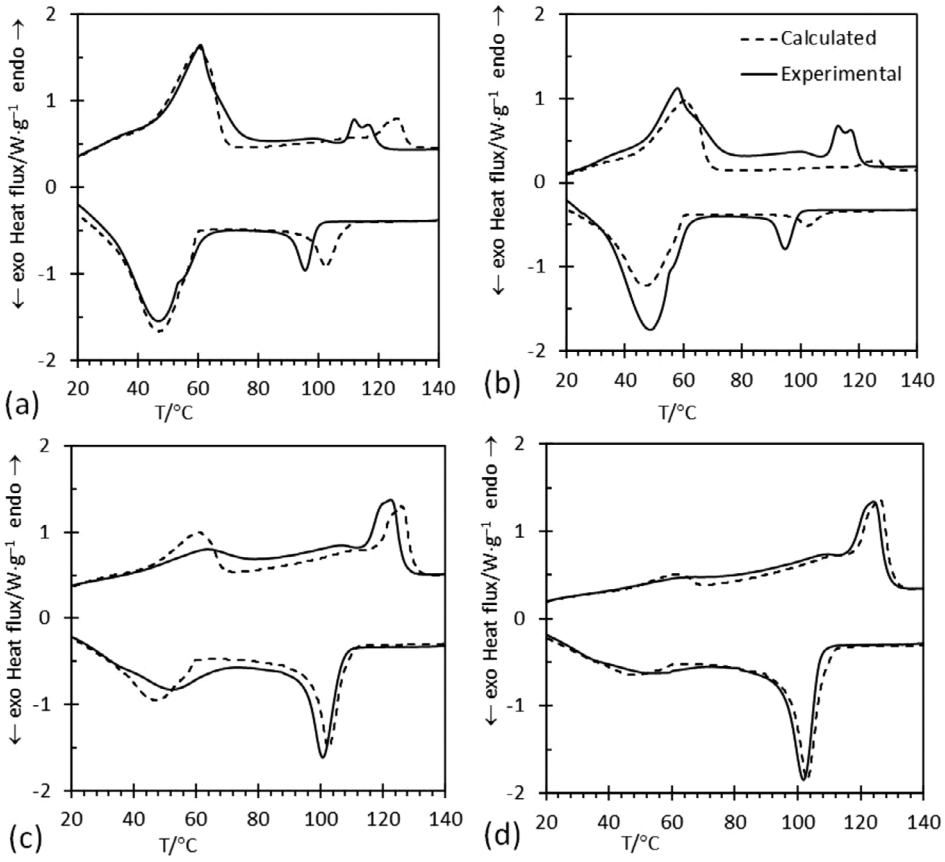

Figure 8. Plot of experimental and predicted melting and crystallization curves for wax/LLDPE blends. The compositions are a) 70/30, b) 50/50, c) 30/70, and d) 10/90.

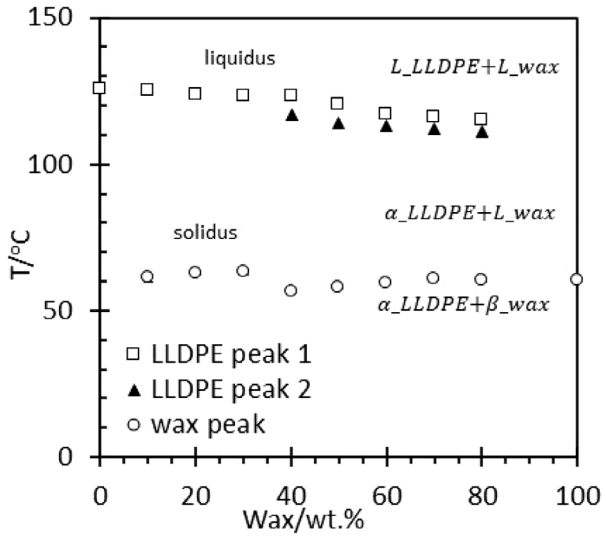

Figure 9. Plot of peak melting temperature as a function of wax/LLDPE at various blend compositions.

wax, the molten wax coexists with solid LLDPE until the liquidus temperature is reached.

The depression of the melting temperature of the LLDPE phase is an indicator of miscibility or partial miscibility of the wax and the LLDPE in the melt. The depression of the melting temperature is likely determined by entropy of mixing effects. Moreover, taking into consideration the occurrence of the bimodal curve distribution, these results suggest that there is a portion of the LLDPE that crystallizes at a lower temperature, while a portion of the wax crystallizes at a higher temperature. This tendency of the wax to act as a plasticizer in the wax/LLDPE binary mixture was previously reported.[7] Moreover, it is well known that, although LLPDE consists predominately of high temperature linear chain molecules, it may have relatively lower melting segments due to the random nature of copolymerization. As a result, the chain segments with a lower melting temperature are more compatible with the shorter chain molecules constituting the wax. Further work is necessary to confirm this speculation. However, it does provide a rational explanation for the observed degree of compatibility indicated by the apparent cocrystallization of the two components.

2.5. Enthalpy of Melting Obtained from Dynamic Temperature Scans

The effect of wax content on the melting enthalpy, ΔH, corresponding to the wax-rich phase and LLDPE-rich phase are shown in **Figure 10**a. The normalized melting enthalpy was determined by the integration of the area under the melting peak and was compared to the theorical melting enthalpy according to Equation (7)

$$\Delta H = w_1 \Delta H_1 + w_2 \Delta H_2 \tag{7}$$

where w represents mass fraction and 1 & 2 represents component 1, wax, and component 2, LLDPE. A strong deviation from the mass-based linear blending rule with the composition was observed. This occurrence was more evident with the wax than the LLDPE. This indicates a strong molecular chain interference in the crystallization process of both components. Consequently, the degree of crystallinity, X, of the blends was calculated from the obtained melting enthalpies as follows

$$X = \Delta H_m / w_i \Delta H_m^0 \tag{8}$$

The standard heat of fusions the pure LLDPE and wax were taken as 293 and 240 J g^{-1}, respectively.[5] The results are presented in Figure 10b. The total crystallinity based on the wax-rich phase increased nearly-linearly with increasing wax fraction. The total crystallinity due to the LLDPE-rich phase is relatively constant up to 20 wt% wax. However, with increasing wax fractions, a gradual reduction that reaches a minimum at 70 wt.% wax and then starts to increase reaching the highest degree of crystallization at 80 wt% wax compositions is observed. The DSC cooling scan from Figure 7b showed that, at the crystallization temperature of the LLDPE phase, the wax-rich phase is in the molten state. This can affect the overall crystallization process of the LLDPE phase. These results indicate that crystallization of a fraction of LLDPE-rich phase is not favored with increasing wax fractions. The presence of the low molecular mass wax increases the free volume in the system, thereby reducing the viscosity of the molten liquid. It was anticipated that this would enhance the mobility of the polymer chains facilitating reorganization and their incorporation into crystallites. Clearly, this was not the case at low- and intermediate- wax fractions. However, it was observed for the 80 wt% wax composition. At this point, it was not clear why the LLDPE crystallization was inhibited at intermediate-wax content.

2.6. Melt Viscosity

Figure 11 shows the effects of wax content on the melt viscosity measured at different shear rates and a temperature of 170 °C. Newtonian behavior is observed up to applied shear rates of 250 s^{-1}. As expected, the apparent viscosity decreased with increasing wax content of the blend. This suggests that the presence, of the low melting wax, increases the overall mobility of the polymer chain molecules in the blend.

Figure 12 plots the zero-shear viscosity versus the fraction wax in the blends. In the context of this study, the wax can be considered to be a low-molecular mass oligomer of the linear low-density polyethylene. Below a critical shear rate, the melt viscosity of polymers show Newtonian behavior characterized by the zero-shear viscosity, as is shown in Figure 12. The Rouse model predicts that this zero-shear viscosity should be proportional to the molecular mass.[8] It is expected that shorter chain molecules, below the critical molecular mass of entanglement, will display Newtonian behavior, i.e., as is the case for the wax. However, long-chain molecules are in a state of entanglement in the melt. This leads to significantly higher viscosities as only cooperative molecular motion is required.[26] The study by Friedman and Porter[27] confirmed that the zero-shear viscosity of such a series of oligomers, polymers, and even their blends, depends uniquely on the weight average molecular mass. Therefore, the

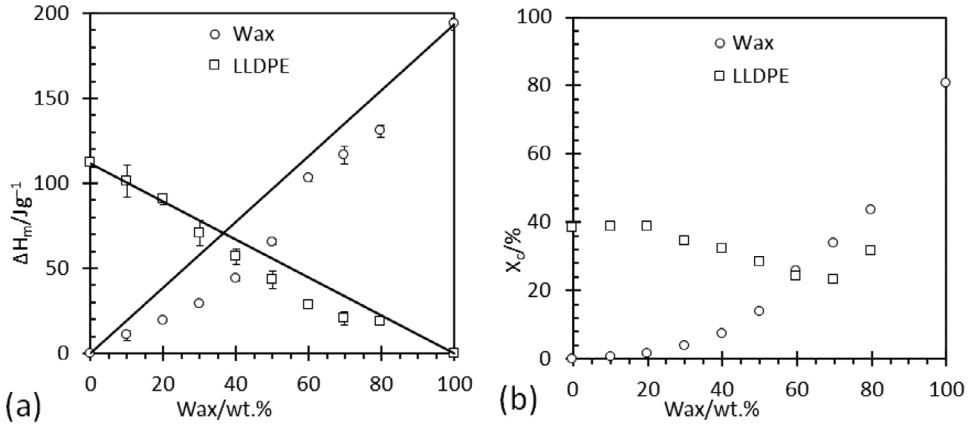

Figure 10. Plot of a) Melting enthalpies and b) degree of crystallinity as a function of wax/LLDPE at various blend compositions.

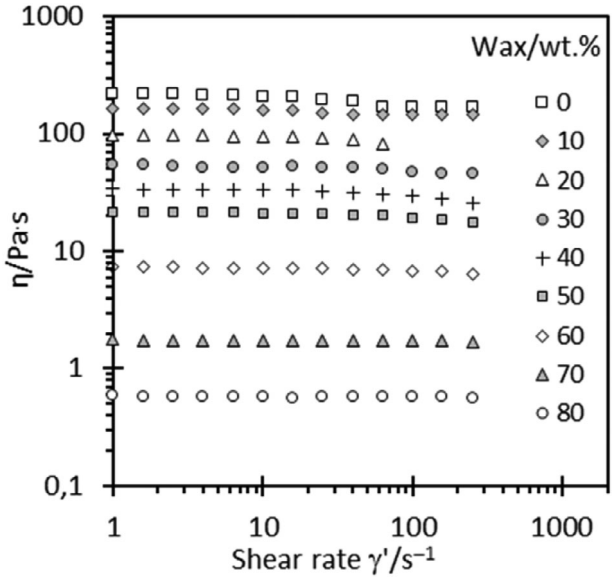

Figure 11. Viscosity flow curves of neat LLDPE and wax/LLDPE at various blend composition.

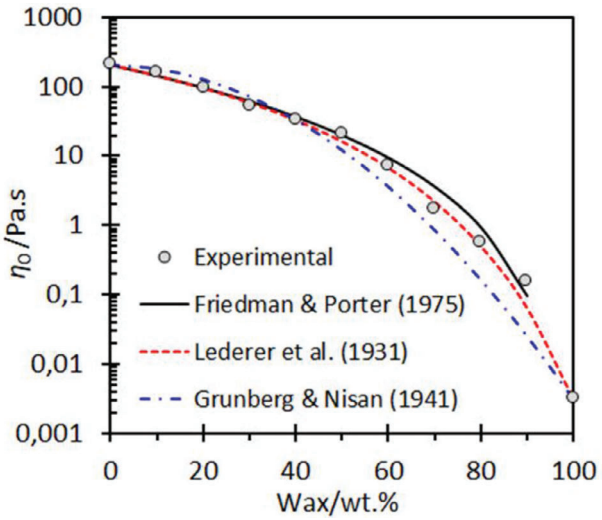

Figure 12. Experimental zero-shear viscosity as a function of wax/LLDPE in comparison to few empirical viscosity blending models at various blend composition.

molecular mass dependence of the zero-shear viscosity can be summarized as follows[26,27]

$$\eta = K_o M_w \quad M_w < M_c \tag{9}$$

$$\eta = K_p M_w^{\alpha} \quad M_w > M_c \tag{10}$$

where K_o and K_p are constants which are dependent on the temperature and the polymer system under investigation. The exponent α takes on the universal value of 3.4 for linear polymers. The breakpoint is defined by M_c, the critical molecular mass above which chain entanglement ensues. The critical molecular mass of polyethylene is ≈3800 Da.[28] Consequently, for the viscosity of polymer blends, with the weight-average molecular mass exceeding M_c, the following mixing rule applies[27]

$$\eta = K_p\left(w_1 M_{w1} + w_2 M_{w2}\right)^{3.4} \tag{11}$$

This curve is plotted in Figure 12 with the value of $K_p = 9.91 \times 10^{-17}$ established from the measured zero-shear viscosity for the polymer melt and its weight-average molecular mass of 245.7 kDa. This is a fully predictive model for blend of the Fischer–Tropsch wax with LLDPE featuring a relatively high molecular mass. The agreement with the experimental results is reasonably good. Empirical correlations were also considered including the Lederer–Roegiers model[29,30] which is recommended for predicting the viscosity of lubricant blends[31]

$$\ln \eta = \left(w_1 \ln \eta_1 + \beta w_2 ln\ \eta_2\right) / \left(w_1 + \beta w_2\right) \tag{12}$$

Least-squares data regression yielded an excellent data fit with the adjustable parameter taking the value $\beta = 3.375$.

A less satisfactory fit was achieved using a modified version of the Grunberg and Nissan[32] model

$$\ln \eta = w_1^2 \ln \eta_1\ 2w_1 w_2 ln \eta_{12} + w_2^2 \ln \eta_2 \tag{13}$$

In this case, the least squares regression yielded, for the interaction viscosity, a value equal to $\eta_{12} = 191.8$ Pa s. The curves predicted by both these models are also shown in Figure 12. Another empirical model is one due to[33]

$$\eta = \eta_1 w_1^2 + 2\eta_{12} w_1 w_2 + \eta_2 w_2^2 \quad (14)$$

However, this model was incapable of reproducing the experimental data trends.

3. Conclusion

The thermal and rheological properties of blends, of a low molecular mass Fischer–Tropsch wax with a linear low-density polyethylene, were investigated. Optical microscopic monitoring of isothermal crystallization, of the LLDPE phase, showed that adding wax decreased the size of the spherulites. Beyond 50 wt% wax, it was not possible to distinguish the spherulites at the magnification applied (×25). The ultimate melting temperature of the LLDPE phase was 137 °C. It decreased progressively with increase in wax content reaching 125 °C at 80 wt% wax. The Hoffman–Weeks parameter was independent of blend composition. This indicates that the dynamics of the lamellar thickening process, for the LLDPE crystallites, was not affected by the presence of the wax.

Isothermal crystallization kinetics, obtained in DSC studies, were modelled using a generalized logistic equation. The crystallization rate versus temperature approached a Gaussian distribution. For the blend containing 70 wt% LLDPE, the characteristic temperature where the crystallization rate reached a maximum was 97.8 °C.

Comparing the dynamic scanning calorimetry traces for the blends to those of the neat components showed the following: a high-temperature shoulder developed in the exotherm for the wax-rich phase, while the LLDPE melting changed into a bimodal event. Both observations are consistent with cocrystallization of a portion of the wax with the LLDPE and vice versa. However, the overall enthalpy of crystallization was less than expected from the linear blending rule. The reduction in the degree of crystallization achieved was more pronounced for the LLDPE portion indicating that the presence of the wax interfered. The effect of blend composition on the zero-shear viscosity, measured at 170 °C was adequately reflected by the Friedman and Porter model. This implies complete compatibility of the components in the molten state at this temperature. However, a slightly better data fit was possible with the Lederer–Roegiers empirical mixture model.

Overall, the results indicate full miscibility of the wax and the LLDPE in the melt and partial cocrystallization in the solid state. In the dynamic DSC scan, the near complete absence of a wax-like melting peak for the blend containing 10 wt% wax suggests complete miscibility at that concentration.

4. Experimental Section

Materials: High-flow LLDPE grade M500026 was supplied by Sabic South Africa (Pty) Ltd. According to the manufacturer, this LLDPE grade had a melt index of 50 g/10 min @ 190 °C/2.16 kg and a density of 926 kg m^{-3}. This polymer was milled into a powder (< 400 μm) by Dream Weaver, South Africa. The number-average molecular mass (M_n) and weight-average molecular mass (M_w) of this LLDPE grade were 26.5 and 92.4 kDa, respectively. Sasol supplied wax M3B in the form of pellets. The corresponding M_n and M_w values were 490 and 493 Da, respectively. An amorphous commercial poly(D-lactic acid) grade, which featured 11.3% D-units was used as a reference material. The M_n, M_w, and polydispersity of this material were 46.8, 147.0, and 3.15 kDa, respectively.

Sample Preparation: Wax/LLDPE blends were prepared by extrusion compounding on a ThermoFischer TSE 24 corotating twin-screw compounder (24 mm Φ, 30 L/D). The die had a single exit hole with a diameter of 5.5 mm. The screw speed was set at 50 rpm. The temperature profile was set as follows, 60/110/140/170/170/170/170 °C. Wax/LLDPE samples were prepared by mixing predetermined quantities of the wax and the polyethylene powders in increments of 10 wt%. The blend containing 90 wt% wax was not prepared due to low melt viscosity posing processing problems.

Characterization Techniques—Hot Stage Polarized Optical Microscopy (POM): The solidification of wax/LLDPE melts was studied with a Leica DM2500M optical microscopy fitted with a Linkam Scientific CSS450 heating stage. Images were recorded with a Leica DFC420 digital camera. The optical micrographs were obtained under polarized light with a 1 λ retarder plate. Samples were placed on the heating stage and covered with a glass slide to ensure that a thin molten film was obtained. The thin sample was heated from room temperature to 170 °C at a rate of 10 °C min^{-1}, then held there for 5 min. Thereafter, the sample was cooled to a selected isothermal crystallization temperature, 65 °C for pure wax and 100 °C for the LLDPE and the blends. During this time, micrographs of the crystalline structure were captured at one-minute intervals at 2.5×, 10×, and 20× magnification.

The equilibrium melting temperature T_m^o of the polymer-rich phase was determined according to the procedure described by Martínez-Salazar et al.[34] Initial programme temperature of 170 °C and subsequent holding for 5 min was chosen to ensure complete melting of the crystals and removal of any residual crystal nuclei. Next, the sample was cooled to the selected isothermal crystallization temperature, T_c, at a rate of 30 °C min^{-1}. Four crystallization temperatures in the range of 105–120 °C were selected. Crystal growth was observed, after 5 min intervals at the isothermal crystallization temperature, sample was reheated at a rate of 10 °C min^{-1}. The melting temperature, T_m, was taken to correspond to the temperature where the last crystal disappeared, i.e., melted.

Characterization Techniques—Differential Scanning Calorimetry (DSC): Thermal analysis was performed on a Perkin Elmer DSC 4000 analyzer. The samples (15 ± 1 mg) were crimped in 50 μL aluminum pans with lids. Nitrogen gas, flowing at a rate of 20 mL min^{-1}, ensured that an inert atmosphere was maintained. The thermal history of each sample was erased by holding it for 5 min at 170 °C.

The isothermal crystallization behavior of the polymer was investigated in the temperature range 98–106 °C. The experiments commenced by cooling the molten sample at 60 °C min^{-1} down to the desired crystallization temperature. The measured response included an artefact due to the dynamic response of the instrument. This was removed by subtracting the measured response obtained using a run according to the same protocol with the poly(D-lactic acid) as the sample material. This amorphous polymer was chosen as it had no thermal transitions in the temperature range of interest.

Nonisothermal crystallization was studied by cycling the temperature between 0 to 170 °C at a scan rate of 10 °C min^{-1}. The data obtained during the second heating and cooling scans were used to determine the peak melting temperature, the peak crystallization temperature and the enthalpy's associated with the melting and crystallization phase transitions.

Characterization Techniques—Rheometry: Rheological measurements were performed on an Anton Paar MCR301 rheometer in a cone-and-plate configuration with a 0.5° cone angle and a diameter of 50 mm. The experiments were conducted isothermally at a temperature of 170 °C. Time was allowed for the samples to melt before squeezing to a gap set at 51 μm. The melt was presheared at 5 s^{-1} for 1 min followed by 1 min at rest. The viscosity data were collected at applied shear rates of 0.01 to 250 s^{-1}.

Acknowledgements

Generous financial support from Sasol is gratefully acknowledged. Sasol research grant agreement SAP No. 126/20 GT.

Conflict of Interest

The authors declare no conflict of interest.

Author Contributions

All authors contributed to the study conception and design. Material preparation, data collection performed by T.M. Analysis of data were performed by all authors. The first draft of the manuscript was written by T.M. and all authors commented on previous versions of the manuscript. All authors read and approved the final manuscript. All the authors have accepted responsibility for the entire content of this submitted manuscript and approved submission.

Data Availability Statement

The data that support the findings of this study are available from the corresponding author upon reasonable request.

Keywords

cocrystallization, LLDPE, viscosity, waxes

Received: April 20, 2023
Revised: June 26, 2023
Published online: July 12, 2023

[1] T. P. Gumede, *J. Vinyl Addit. Technol.* **2001**, *27*, 469.
[2] L. Radebe, J. Wesley-Smith, W. W. Focke, S. Ramjee, *J. Polym. Eng.* **2023**, *43*, 80.
[3] M. E. Sotomayor, I. Krupa, A. Várez, B. Levenfeld, *Renewable Energy* **2014**, *68*, 140.
[4] H. S. Mpanza, A. S. Luyt, *S. Afr. J. Chem.* **2006**, *59*, 48.
[5] F. Chen, M. P. Wolcott, *Europ. Polym. J.* **2014**, *52*, 44.
[6] F. Chen, M. P. Wolcott, *Sol. Energy Mater Sol Cells.* **2015**, *137*, 79.
[7] T. P. Gumede, A. S. Luyt, R. A. Pérez-Camargo, A. Iturrospe, A. Arbe, M. Zubitur, A. Mugica, A. J. Müller, *J. Polym. Sci., Part B: Polym. Phys.* **2016**, *54*, 1469.
[8] J. Dealy, R. Larson, *Structure and Rheology of Molten Polymers: From Structure to Flow Behaviour and Back Again*, Chiron Media, Wallingford, UK **2006**.
[9] G. L. Wilkes, *J. Chem. Educ.* **1981**, *58*, 880.
[10] C. Liu, J. Wang, J. He, *Polymer* **2002**, *43*, 3811.
[11] K. Ho, L. Kale, S. Montgomery, *J. Appl. Polym. Sci.* **2002**, *85*, 1408.
[12] T. Mhlabeni, C. Ngobese, S. Ramjee, W. Focke, *J. Vinyl Addit. Technol.* **2023**, 1. https://doi.org/10.1002/vnl.21984.
[13] J. Martínez-Salazar, M. S. Cuesta, J. Plans, *Polymer* **1991**, *32*, 2984.
[14] B. P. Saville, *Polarized Light: Qualitative Microscopy, in Applied Polymer Light Microscopy*, (Ed: D. A. Hemsley) Springer, Dordrecht, Netherlands **1989**, pp. 111-149. https://doi.org/10.1007/978-94-011-7474-9_4.
[15] H. D. Keith, F. J. Padden, *Macromolecules* **1996**, *29*, 7776.
[16] J. D. Hoffman, L. J. Frolen, G. S. Ross, J. I. Lauritzen, *J. Res. Natl. Bur. Stand., Sect. A* **1975**, *79A*, 671.
[17] J. J. Weeks, *J. Res. Natl. Bur. Stand., Sect. A* **1963**, *67A*, 441.
[18] H. Mohammadi, M. Vincent, H. Marand, *Polymer* **2018**, *146*, 344.
[19] W. W. Focke, I. Van Der Westhuizen, N. Musee, M. T. Loots, *Sci. Rep.* **2017**, *7*, 2234.
[20] A. M. Díaz-Díaz, J. López-Beceiro, Y. Li, Y. Cheng, R. Artiaga, *J. Therm. Anal. Calorim.* **2021**, *145*, 3125.
[21] A. V. Hill, *J. Physiol.* **1910**, *40*, 4.
[22] M. Avrami, *J. Chem. Phys.* **1939**, *7*, 1103.
[23] I. Krupa, A. S. Luyt, *Polymer* **2001**, *42*, 7285.
[24] T. N. Mtshali, C. G. Van Sittert, V. Djoković, A. S. Luyt, *J. Appl. Polym. Sci.* **2003**, *89*, 2446.
[25] H. S. Mpanza, A. S. Luyt, *Polym. Test.* **2006**, *25*, 436.
[26] T. G. Fox, P. J. Flory, *J. Phys. Chem.* **1951**, *55*, 221.
[27] E. M. Friedman, R. S. Porter, *Trans. Soc. Rheol.* **1975**, *19*, 493.
[28] D. Nichetti, I. Manas-Zloczower, *J. Rheol.* **1998**, *42*, 951.
[29] L. Fetters, D. Lohse, R. Colby, in *Physical Properties of Polymers Handbook*, (Ed: J. E. Mark), Springer, New York **2007**. https://doi.org/10.1007/978-0-387-69002-5_25.
[30] E. Lederer, *Kolloid-Beihefte* **1931**, *34*, 270.
[31] M. Roegiers, L. Roegiers, La viscosité des mélanges de“ fluides normaux”. Submitted in Gand by Impr AA Hoste. **1947**.
[32] B. Zhmud, *Lube-Tech* **2014**, *93*, 22.
[33] L. Grunberg, A. S. Nissan, *Nature* **1949**, *164*, 799.
[34] R. K. Hind, E. McLaughlin, A. R. Ubbelohde, *Trans. Faraday Soc.* **1960**, *56*, 328.

